Inorganic Chemistry

Article

pubs.acs.org/IC

$BaAu_2P_4$: Layered Zintl Polyphosphide with Infinite $^1_\infty(P^-)$ Chains

James Fulmer,[†] Derrick C. Kaseman,[‡] Juli-Anna Dolyniuk,[†] Kathleen Lee,[†] Sabyasachi Sen,[‡] and Kirill Kovnir*,[†]

[†]Department of Chemistry and [‡]Department of Chemical Engineering and Materials Science, University of California, Davis, One Shields Avenue, Davis, California 95616, United States

Supporting Information

ABSTRACT: Barium gold polyphosphide $BaAu_2P_4$ was synthesized from elements and structurally characterized by single crystal X-ray diffraction. $BaAu_2P_4$ crystallizes in a new structure type, in the orthorhombic space group *Fddd* (No. 70) with a = 6.517(1) Å, b = 8.867(2) Å, c = 21.844(5) Å. The crystal structure of $BaAu_2P_4$ consists of Au−P layers separated by layers of Ba atoms. Each Au−P layer is composed of infinite $^1_\infty(P^-)$ chains of unique topology linked together by almost linearly coordinated Au atoms. According to Zintl−Klemm formalism, this compound is charge balanced assuming closed shell d^{10} configuration for Au: $Ba^{2+}(Au^+)_2(P^-)_4$. Magnetic and solid state NMR measurements together with quantum-chemical calculations reveal diamagnetic and semiconducting behavior for the investigated polyphosphide, which is as expected for the charged balanced Zintl phase. Electron localization function and crystal orbital Hamilton population analyses reveal strong P−P and Au−P bonding and almost nonbonding Au−Au interactions in $BaAu_2P_4$.

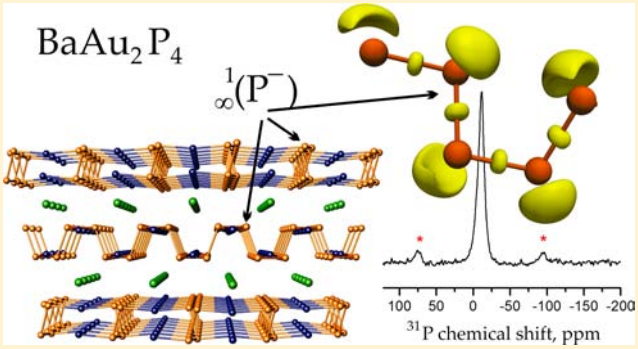

INTRODUCTION

Phosphorus is known to form numerous polyphosphide anions.[1] The topology and dimensionality of such polyanions is dictated by (i) the tendency of phosphorus atoms to realize an electron octet by utilizing their own valence electrons along with the electrons provided by surrounding metal cations; and (ii) the number, size, and preferred coordination of metal cations. This results in a plethora of different chemical compositions, crystal structures, and a variety of physical properties. The fascinating chemistry of binary and ternary metal polyphosphides was reviewed by von Schnering and Hönle 25 years ago.[2] A combination of two metals with different chemical natures has proven to be an effective way to produce new polyphosphides with unprecedented phosphorus polyanion topologies.[3−10]

In our search for new semiconducting phosphides with potential thermoelectric applications we came across a new barium gold phosphide $BaAu_2P_4$. Thermoelectric materials are capable of converting heat into electrical energy and vice versa.[11] They can be used for a wide range of applications such as Freon-free refrigerators and AC units, as well as waste heat and direct solar thermal energy converters.[12] To be effective, thermoelectric materials are expected to exhibit low values of both electrical resistivity and thermal conductivity. The peculiarities of the crystal and electronic structures of highly anisotropic layered polyphosphides with narrow band-gaps make them potentially effective thermoelectric materials. In this work, we report the synthesis of the $BaAu_2P_4$, which crystallizes in a new structure type with a unique topology of infinite phosphorus chains $^1_\infty(P^-)$. We have characterized this compound by means of X-ray diffraction, scanning electron microscopy (SEM)-energy dispersive X-ray (EDX) micro-analysis, solid state ^{31}P nuclear magnetic resonance (NMR) spectroscopy, magnetic properties measurements, as well as quantum-chemical calculations including electron localization function (ELF) analysis.

EXPERIMENTAL SECTION

Single phase samples of $BaAu_2P_4$ were prepared by solid-state reactions. All manipulations with the initial materials were performed inside an argon-filled glovebox ($p(O_2)$, $p(H_2O) \leq 1$ ppm). The starting materials, metallic barium (Sigma-Aldrich, 99.9%), gold powder (Alfa Aesar, 99.96%), gold(I) chloride (Sigma-Aldrich, 99%), and red phosphorus (Alfa Aesar, 99%), were used as received. Single phase samples of $BaAu_2P_4$ were produced from elemental Ba, Au, and P. Reagents were mixed in a stoichiometric ratio, placed in glassy-carbon crucibles, and subsequently sealed inside evacuated silica ampules. The ampules were heated to 1173 K over 17 h and annealed at that temperature for 140 h. The products were ground and annealed again for 140 h under the same conditions. Annealed samples contained numerous metallic plate-like crystals, which were stable in air for at least several months and resistant to a 72 h treatment with concentrated hydrochloric acid.

Additionally, single crystals for structural analysis have been synthesized using AuCl as a flux. Hereby, Ba, AuCl, and P were mixed in a 2:2:4 molar ratio and annealed at 1173 K for 140 h. Any

Received: March 8, 2013
Published: June 4, 2013

   dx.doi.org/10.1021/ic400584w | *Inorg. Chem.* 2013, 52, 7061−7067

barium chloride formed during synthesis was removed by washing the sample with water.

X-ray Powder Diffraction and Elemental Analysis. The samples were characterized by powder X-ray diffraction (XRD) using a Bruker D8 Advance diffractometer employing CuK_α radiation (Supporting Information, Figure SI 1). Elemental analysis of selected single crystals was carried out on a Hitachi S4100T scanning electron microscope (SEM) with energy-dispersive X-ray (EDX) microanalysis (Oxford INCA energy) (Supporting Information, Figure SI 1). Sample analysis confirmed the presence of only Ba, Au, and P in the samples. Because of the overlap of Au and P lines, the EDX analysis was semiquantitative. The experimental ratio of (Au+P)/Ba, 6.2, was close to what was expected from the single crystal diffraction determined ratio of 6.

Single Crystal X-ray Diffraction. Data were collected at room temperature using Bruker AXS SMART diffractometer with an APEX-II CCD detector. The data set was recorded as ω-scans with 0.3° step width and integrated with the Bruker SAINT software package. The data set was indexed in an orthorhombic face-centered unit cell. Systematic extinctions clearly indicate *Fddd* (No.70) as the only possible space group. An analytical absorption correction was applied using face-indexing of the crystal. The solution and refinement of the crystal structure were carried out using the SHELX suite of programs.[13] The structure was solved in the *Fddd* space group, and the final refinement was performed using anisotropic atomic displacement parameters for all atoms. A summary of pertinent information relating to unit cell parameters, data collection, and refinements is provided in Table 1, and atomic parameters and interatomic distances are provided in Tables 2−3.

Table 1. Data Collection and Structure Refinement Parameters for $BaAu_2P_4$[a]

space group	*Fddd* (no. 70)	ρ [g cm^{-3}]	6.895
temp. [K]	293(2)	μ [mm^{-1}]	53.420
a [Å]	6.517(1)	θ [deg.]	$3.73 < \theta < 26.96$
b [Å]	8.867(2)	data/parameters	346/18
c [Å]	21.844(5)	R_1	0.017
V [Å^3]	1262.3(5)	wR_2	0.034
Z	8	goodness-of-fit	1.075
λ [Å]	0.71073	diff. peak and hole [e/Å^3]	1.57 and −1.02

[a]Further details of the crystal structure determination may be obtained from Fachinformations-zentrum Karlsruhe, D-76344 Eggenstein-Leopoldshafen, Germany, by quoting the depository number CSD-425778.

Table 2. Atomic Coordinates and Equivalent Displacement Parameters for $BaAu_2P_4$

atom	Site	x/a	y/b	z/c	U_{eq}[a]
Ba	8*a*	$^1/_8$	$^1/_8$	$^1/_8$	0.0185 (1)
Au	16*g*	$^1/_8$	$^1/_8$	0.28814(1)	0.0134(1)
P	32*h*	0.4371(2)	0.2592(2)	0.29723(6)	0.0131(3)

[a]U_{eq} is defined as one-third of the trace of the orthogonalized U_{ij} tensor.

Solid State ^{31}P Nuclear Magnetic Resonance (NMR) Spectroscopy. The ^{31}P magic angle spinning (MAS) NMR spectrum of polycrystalline $BaAu_2P_4$ was collected using a Bruker Avance 500 spectrometer operating at a magnetic field of 11.7 T, ^{31}P resonance frequency = 202.4 MHz. A crushed $BaAu_2P_4$ sample was placed in a ZrO_2 rotor and spun at 17 kHz in a Bruker 2.5 mm MAS probe. The one-pulse ^{31}P MAS NMR spectrum was obtained using a $\pi/4$ pulse (1 μs) and a recycle delay of 60 s. A total of 124 free induction decays were averaged and Fourier transformed to obtain the spectrum. A ^{31}P static spectrum of the sample was also collected using a Bruker 7 mm MAS probe. The crushed sample was placed in a ZrO_2 rotor, and the spectrum was collected using a $\pi/4$ pulse (2 μs) and a recycle delay of 60 s. A total of 100 free induction decays were averaged and Fourier transformed to obtain the static spectrum. The static line shape was simulated using the software DMfit.[14] The ^{31}P chemical shift was externally referenced to that of aqueous 85% H_3PO_4.

Table 3. Selected Interatomic Distances (Å) and Angles (deg) for $BaAu_2P_4$

atoms	distance	atoms	angle
Au−P	2.365(1)×2	∠ P−Au−P	170.37(6)
Au−Au	3.2165(6)×2	∠ Au−Au−Au	117.59(2)
P−P	2.207(3)	∠ P−P−P	101.72(8)
P−P	2.227(3)		
Ba−Au	3.3419(5)×4		
Ba−Au	3.5637(9)×2		
Ba−P	3.476(1)×4		
Ba−P	3.828(1)×4		

Magnetic Properties. The temperature dependence of the magnetic susceptibility was measured in the applied field of 0.1 T using the commercial Magnetic Property Measurement System (Quantum Design MPMS). A corresponding diamagnetic correction for the contribution of the sample container was applied by measuring an empty sample container under similar conditions.

Quantum-Chemical Calculations. Density functional band structure calculations using a full potential all-electron local orbital code FPLO (version fplo7.00−28) within the local density approximation (LDA) were performed.[15] The Perdew−Wang parametrization of the exchange-correlation potentials was employed.[16] The density of states (DOS) and band structures were calculated after convergence of the total energy on a dense k-mesh with 32 × 32 × 32 points, with 4505 irreducible k-points. Additionally, electronic structure calculations and bonding analysis were carried out using the tight binding−linear muffin tin orbitals−atomic sphere approximation (TB−LMTO−ASA) program package.[17] The Barth−Hedin exchange potential was employed for LDA calculations. The radial scalar-relativistic Dirac equation was solved to obtain the partial waves. A basis set containing Ba(6s,5d,4f), Au(6s,6p,5d), and P(3s,3p) orbitals was employed for a self-consistent calculation, with Ba(6p), Au(5f), and P(3d) functions being downfolded. For bonding analysis, the energy contributions of all electronic states for selected atom pairs were evaluated with a crystal orbital Hamiltonian population (COHP) analysis.[18] Integration over all filled states yielded −ICOHP values as measures of relative overlap populations. The electron localization function (ELF, η)[19] was evaluated with modules implemented within the TB−LMTO−ASA program package. The ParaView program was used for visualization of ELF isosurfaces.[20]

RESULTS AND DISCUSSION

Synthesis. The formation of $BaAu_2P_4$ was first observed during studies of the thermal stability of the clathrate phase $Ba_8Au_{16}P_{30}$.[21] Subsequently, synthesis of the single phase sample of $BaAu_2P_4$ was performed by annealing the mixture of elements at 1173 K. The presence of a small admixture (<5%) of metallic gold cannot be excluded because of the overlap of Au and $BaAu_2P_4$ diffraction peaks as well as texturing of the latter compound (Supporting Information, Figure SI 1). The optimal temperature for synthesizing $BaAu_2P_4$ appeared to be 1173 K. Increasing the synthesis temperature to 1273 K resulted in the formation of a multiphase sample containing Au, Au_2P_3, barium phosphides, and $BaAu_2P_4$. In turn, reduction of the synthesis temperature to 1123 K led to the formation of mixtures of $Ba_8Au_{16}P_{30}$[21] and $BaAu_2P_4$.

Crystal Structure. $BaAu_2P_4$ crystallizes in a new structure type. The crystal structure can be described as $[Au_2P_4]^{2-}$ layers separated by Ba^{2+} cations (Figure 1a). Barium atoms are coordinated by six gold and eight phosphorus atoms forming a

dx.doi.org/10.1021/ic400584w | Inorg. Chem. 2013, 52, 7061−7067

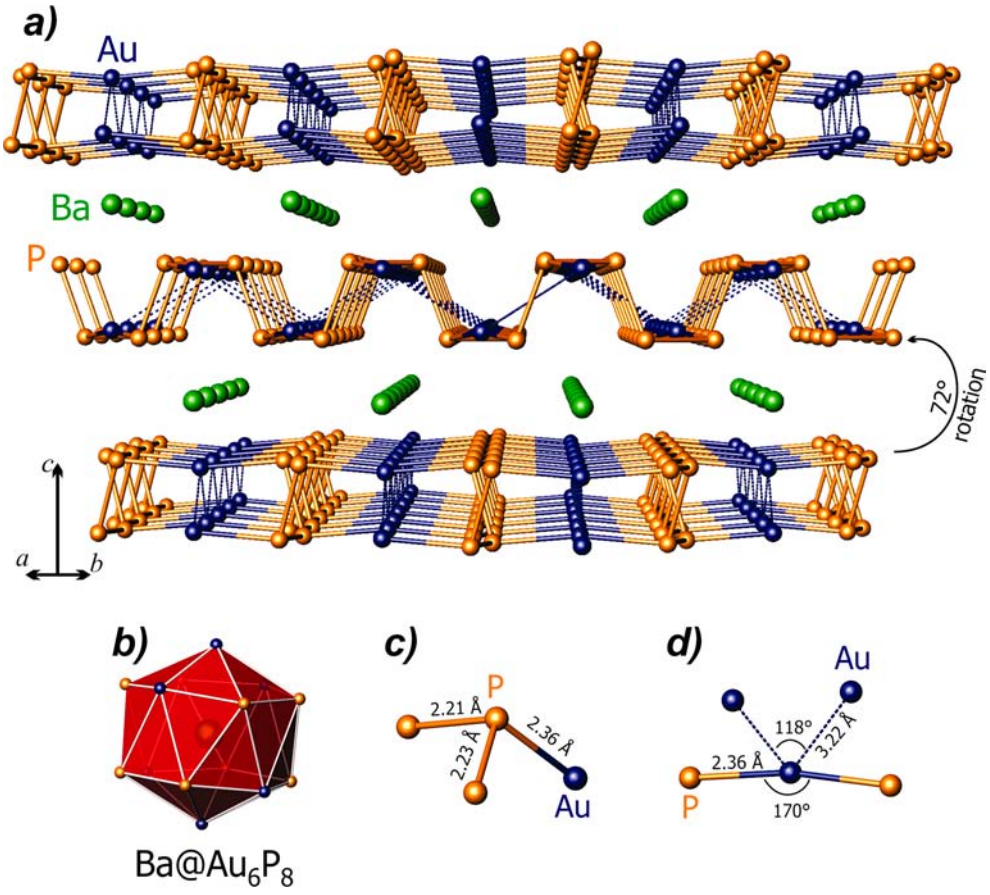

Figure 1. Crystal structure of $BaAu_2P_4$: (*a*) general view; local coordination of (*b*) Ba, (*c*) P, and (d) Au atoms.

distorted bicapped hexagonal antiprism (Figure 1b). The $[Au_2P_4]^{2-}$ layer is composed of infinite phosphorus chains $^1_\infty(P^-)$ running parallel to each other and linked together with gold atoms. Four identical $[Au_2P_4]^{2-}$ layers are present in the unit cell (Supporting Information, Figure SI 2). Each next layer is shifted and rotated with respect to the previous layer. All phosphorus chains in one layer are parallel to each other. The propagation directions of the phosphorus chains in neighboring layers are rotated by ~72° along [001] axis. The stacking of $[Au_2P_4]^{2-}$ layers is mediated by electrostatic interactions with Ba atoms. Reciprocal lattice images of $BaAu_2P_4$ reveal the presence of diffuse scattering features (Supporting Information, Figure SI 3), which indicates the possibility of stacking disorder.

Each phosphorus atom has a coordination number of three: 2P+1Au (Figure 1c). Each gold atom is almost linearly coordinated (∠P−Au−P is 170°) with two phosphorus atoms at a distance of 2.36 Å. Two more distant gold atoms at 3.22 Å complete the coordination sphere of Au (Figure 1d). A linear coordination for gold atoms with two phosphorus atoms is found in other gold phosphides, like Au_2P_3,[22] K_2AuP,[23] and MAu_2P_2 (M = Hg, Tl, Pb)[8] (Figures 2a-2c). In K_2AuP two more distinct gold atoms, *d*(Au−Au) = 3.08 Å, form a planar rhombus around the central gold atom, ∠Au−Au−Au is 180° (Figure 2a). A similar nearly planar coordination of 2P+2Au atoms is found in MAu_2P_2 (Figure 2c). In Au_2P_3, four gold atoms, *d*(Au−Au) = 2.93 Å and 3.10 Å, complete the coordination of the central gold atom forming a distorted octahedron with all five gold atoms lying in one plane (Figure 2b). In the structure of $BaAu_2P_4$, ∠Au−Au−Au is only 118°

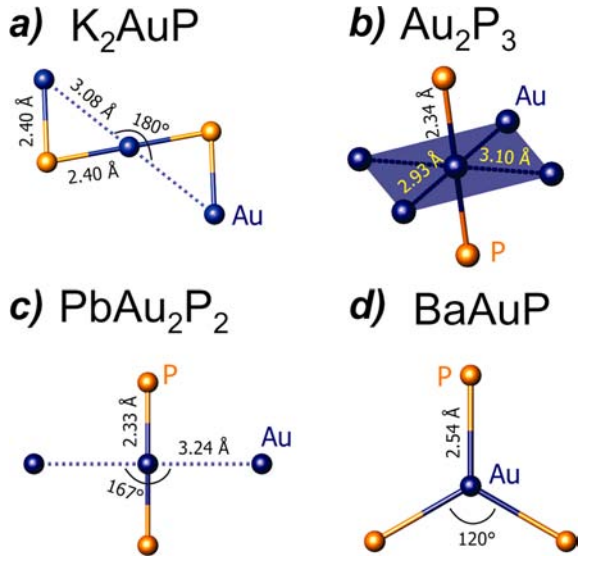

Figure 2. Local atomic coordination of gold atoms in the crystal structures of (*a*) K_2AuP,[23] (*b*) Au_2P_3,[22] (*c*) $PbAu_2P_2$,[8] and (*d*) BaAuP.[24] Note that in the latter case the shortest Au−Au distance is 4.41 Å.

and the $Au@Au_2P_2$ unit has a butterfly shape (Table 3, Figure 1d).

The Ba−Au−P system exhibits high diversity in the local coordination of gold and phosphorus atoms. Besides $BaAu_2P_4$, Nuss and Jansen have reported a BaAuP compound where Au and P atoms have trigonal-planar coordination and no

dx.doi.org/10.1021/ic400584w | *Inorg. Chem.* 2013, 52, 7061−7067

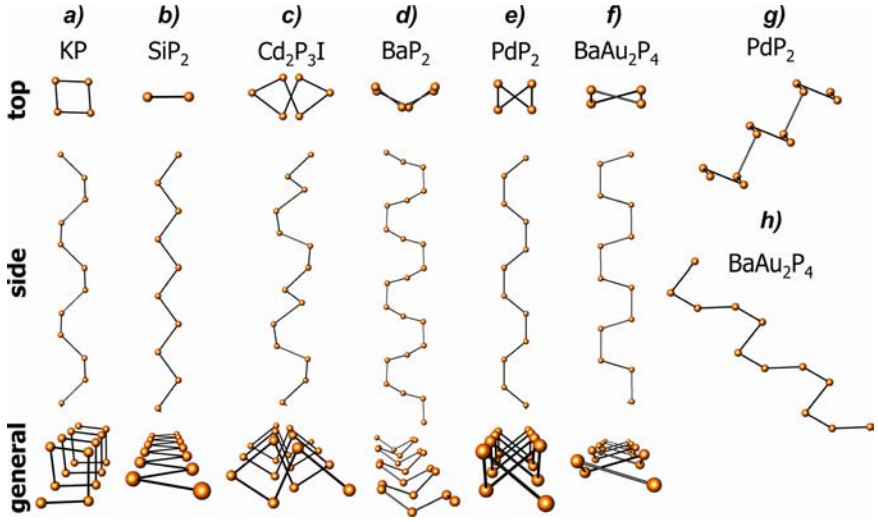

Figure 3. Five types (a–e) of the $^1_\infty(P^-)$ chains found in metal phosphides compared with chains present in (f) $BaAu_2P_4$: top, side, and general view; additional side view of the chains present in (g) PdP_2 and (h) $BaAu_2P_4$.

homoatomic bonds are formed (Figure 2d and Supporting Information, Figure SI 4).[24] We have recently synthesized a clathrate compound $Ba_8Au_{16}P_{30}$ where Au and P atoms are tetrahedrally coordinated, and multiple P–P bonds are present.[21] Another interesting example of a compound containing phosphorus chains linked together by gold atoms was reported by Jeitschko et al. in the compounds MAu_2P_2 (M = Hg, Tl, Pb).[8] In the crystal structures of MAu_2P_2 each phosphorus atom is coordinated by two gold atoms thus forming a three-dimensional framework with M atoms situated in the large channels of this framework (Supporting Information, Figure SI 4).

The infinite phosphorus chains $^1_\infty(P^-)$ have a different topology in MAu_2P_2 and $BaAu_2P_4$. The $^1_\infty(P^-)$ polyanionic phosphorus fragment is typical for various metal polyphosphides such as the monophosphides of alkali metals and the diphosphides of divalent metals. While the local ∠P–P–P is close to a regular tetrahedral angle, $^1_\infty(P^-)$ chains exhibit high configurational and conformational variability, which is dictated by the size and coordination of surrounding cations (Figure 3). Five types of $^1_\infty(P^-)$ chains have been reported so far. From Figures 3e and 3f one may conclude that phosphorus chains in $BaAu_2P_4$ are similar in topology to those found in PdP_2.[25] However, Figures 3g and 3h demonstrate the difference between those chains. In PdP_2, four phosphorus atoms lie in the plane perpendicular to the direction of chain propagation. This leads to the following sequence of torsion angles: 180°–92°–180°–92° (Supporting Information, Table SI 1). In $BaAu_2P_4$, the torsion angles are 180°–38°–180°–38° and no planar fragments perpendicular to the direction of chain propagation are present. To the best of our knowledge, the phosphorus chains present in $BaAu_2P_4$ are unique.

Electronic Structure and Properties. According to the Zintl concept[26,27] $BaAu_2P_4$ is an electron balanced compound and gold exhibits a closed-shell d^{10} electronic configuration. Assuming full electron transfer from Ba and Au cations to phosphorus atoms, each phosphorus atom should form two homonuclear bonds and have two electron lone pairs, thus realizing an electron octet. This would require six electrons per phosphorus atom, that is, a formal oxidation state of −1. The formula of the compound can be written as $(Ba^{2+})(Au^+)_2(P^-)_4$. Band structure calculations support thus assumption (vide infra).

Measurements of the temperature dependence of the magnetic susceptibility reveal the diamagnetic behavior of $BaAu_2P_4$ as expected for a Zintl phase (Figure 4). The

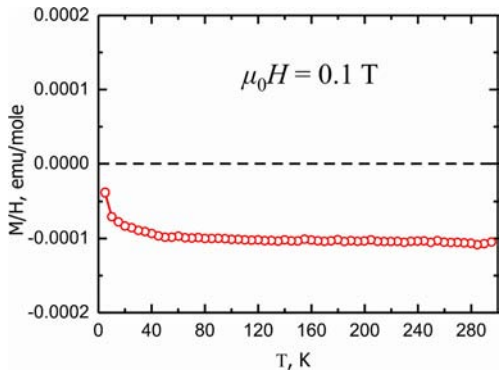

Figure 4. Temperature dependence of the magnetic susceptibility of $BaAu_2P_4$ measured in the DC applied magnetic field of 0.1 T.

diamagnetic contribution can be calculated using Pascal constants for Ba^{2+} (-26×10^{-6} emu/mol), Au^+ (-40×10^{-6} emu/mol), and P^0 (-26.3×10^{-6} emu/mol).[28] The resulting calculated contribution for $BaAu_2P_4$ (-2.1×10^{-4} emu/mol) is slightly smaller than the observed value. Note that no tabulated value for P^- is reported, which may explain the observed discrepancy.

The ^{31}P MAS and static NMR spectra of the polycrystalline $BaAu_2P_4$ sample are shown in Figure 5. The ^{31}P MAS NMR spectrum (Figure 5a) is characterized by a single resonance with an isotropic chemical shift of −11.4 ppm, corresponding to the single crystallographic site of phosphorus in the crystal structure, as discussed above. This chemical shift is well within the typical range for ^{31}P chemical shifts reported in the literature for a wide selection of diamagnetic phosphides and is therefore indicative of the lack of any significant free-electron density at P sites in this compound. Indeed, for electron-balanced Zintl compounds the ^{31}P chemical shift is below +2 ppm.[5a,29–32] For compounds with a partially filled conduction band, that is, metal-like, ^{31}P chemical shifts are much higher.

dx.doi.org/10.1021/ic400584w | Inorg. Chem. 2013, 52, 7061–7067

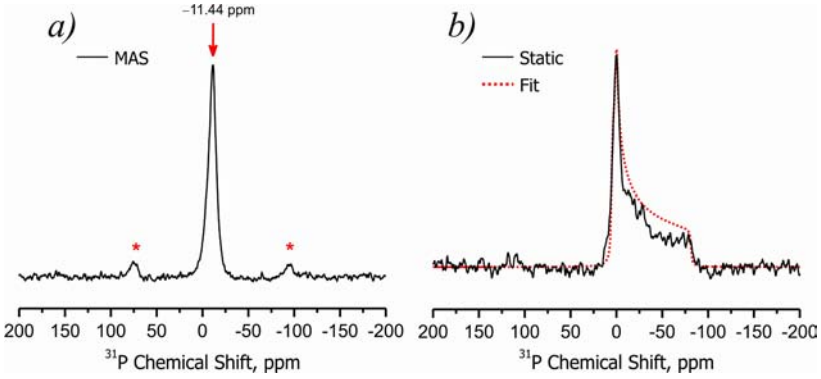

Figure 5. ^{31}P NMR spectra of $BaAu_2P_4$. (*a*) MAS spectrum with spinning sidebands marked with asterisks; (*b*) experimental (solid line) and simulated (dotted line) static spectrum.

For example in the paramagnetic $LaIr_2P_2$, ^{31}P chemical shifts are +709 ppm and +1160 ppm.[33] Such high frequency shifts are caused by either strong Fermi interactions of the nuclear magnetic moments with a nonzero delocalized electron density of unpaired electronic spins or by a Knight shift from conduction electrons.

Additionally, these kinds of interactions lead to significant broadening of the MAS NMR signals. Thus, the paramagnetic transition metal-containing Zintl phase $Ca_{14}MnP_{11}$ exhibits quite broad lines with full width at half-maximum (fwhm) of >200 ppm.[34] The observed chemical shift of −11.44 ppm with a fwhm of 10 ppm (~2 kHz) confirms the diamagnetic electron-balanced nature of $BaAu_2P_4$. Simulation of the static ^{31}P NMR line shape (Figure 5b) yields a chemical shift anisotropy of −56 ppm (~11.3 kHz) and an asymmetry parameter η of ~0.1 implying a nearly uniaxial symmetry of the shielding tensor for the P site. Although not known a priori, the unique axis of symmetry of the ^{31}P shielding tensor may be aligned either along the P−Au bond or along the direction of the electron lone pair on the P atom.

Band structure calculation results obtained by two different methods were similar. The results of the more accurate method, FPLO, are shown in Figure 6. According to the calculations, $BaAu_2P_4$ is a narrow band gap semiconductor with E_g = 0.25 eV. In agreement with the assumptions drawn from applying the Zintl concept, the top of the valence band is composed of P3p orbitals with small contributions from P3s, Au5d, and Au6s orbitals. Contributions from the Au5d orbitals dominate the states in the −2 to −7 eV range. P3s and Au6s contributions are spread over a wide energy range. Ba orbitals contribute mainly to the conduction band.

Results of band structure calculations, magnetic and NMR investigations generally support the conclusion drawn from the simple yet powerful Zintl concept: $BaAu_2P_4$ is a narrow band gap semiconductor. The Zintl concept was developed for main group elements and in general it is not suitable to describe bonding involving d-electrons.[26,27] In the $BaAu_2P_4$ compound there is a relatively short Au−Au interatomic separation of 3.22 Å. To verify whether this corresponds to chemical bonding interaction we have applied ELF analysis (Figure 7).[19,35]

Three main types of attractors were revealed by ELF analysis: attractor ① corresponds to two centered P−P interactions within $^1_\infty(P^-)$ chain, attractor ② corresponds to electron lone pairs located on phosphorus atoms, and attractor ③ corresponds to P−Au interactions. For the latter, the ELF maximum is shifted toward phosphorus atoms, thus confirming

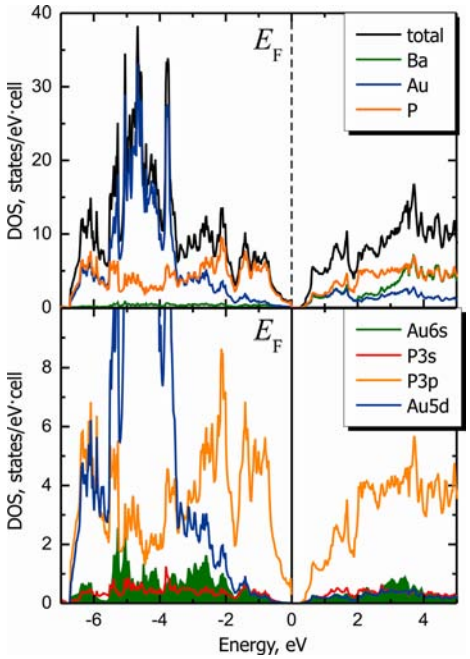

Figure 6. Density of states (DOS) diagram for $BaAu_2P_4$. In the top panel the contributions from Ba, Au, and P are shown in green, blue, and orange, respectively. The bottom panel shows enlarged orbital contributions of P3s (red), P3p (orange), Au5d (blue), and Au6s (green) orbitals.

the assumption about the polarity of the Au−P bond and the partial charge transfer from gold to phosphorus atoms. Figure 7b shows the ELF distribution around the Au_3 fragment in the crystal structure of $BaAu_2P_4$. There is a minimum of ELF distribution on the line connecting two gold atoms, indicating an absence of bonding Au−Au interactions in $BaAu_2P_4$. A similar result was observed for the even shorter Au−Au separation of 2.93 Å in Au_2P_3 where no bonding maxima were revealed by ELF (Supporting Information, Figure SI 5).

In various polyanionic gold-containing compounds Au−Au bonding was analyzed with the help of COHP analysis.[18] This method has limitations for the investigation of multicenter bonds, but is well-suited for two-center bonding and is able to estimate net bonding. A large number of different compounds in the A−Au−M system (A = alkali metal; M = Ga, In, Tl, Sn, Sb, Bi) were characterized by the Corbett's and Miller's groups.[36,37] Most of the group 13 and 14 compounds exhibit metallic properties, but K_2AuSb and K_2AuBi are semi-

dx.doi.org/10.1021/ic400584w | Inorg. Chem. 2013, 52, 7061−7067

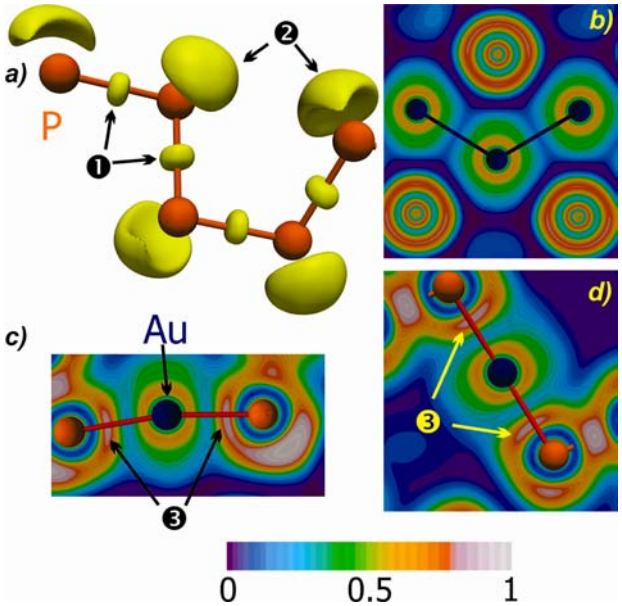

Figure 7. (*a*) 3D isosurfaces of electron localization function (η) for the phosphorus chain in $BaAu_2P_4$ (η = 0.83). Coloring of the electron localization function (η) distributions for slices of the crystal structure of $BaAu_2P_4$: (*b*) Au_3 fragment, (*c, d*) AuP_2 fragment.

conductors.[37] These compounds are isostructural to K_2AuP (vide supra). In the K_2AuSb and K_2AuBi band structures, gold atoms have a significant contribution to the states near the Fermi level, differentiating them from $BaAu_2P_4$ in which the top of the valence band is composed of phosphorus 3p orbitals (Figure 6). COHP curves for different types of interactions in $BaAu_2P_4$ are shown in Figure 8 together with the contribution

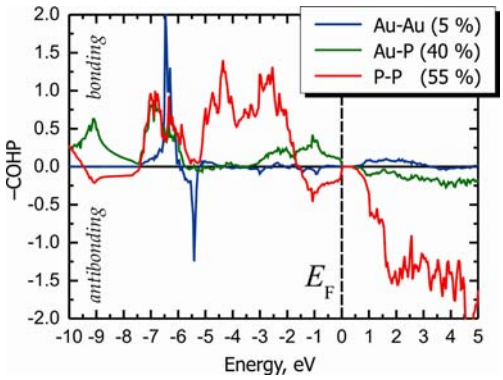

Figure 8. COHP curves for interactions within the polyanionic layer in $BaAu_2P_4$: Au−Au blue line; Au−P green line; P−P red line.

of each COHP to the total bonding. P−P bonding is mainly optimized with a small antibonding contribution around the Fermi level, probably because of the presence of electron lone pairs. Au−P bonding is also optimized with all bonding states below the Fermi level and antibonding ones above the Fermi level. Au−Au bonding holds a small positive net bonding but at the energies from −5 eV to the Fermi level, the contribution of Au−Au bonding is close to zero. The net bonding from −ICOHP are as follows: P−P (~0.9 eV·cell^{-1}·mol^{-1}), Au−P (~1.3 eV·cell^{-1}·mol^{-1}), Au−Au (~0.16 eV·cell^{-1}·mol^{-1}). This corresponds to 40%, 55%, and 5% contributions to the bonding within the polyanionic $[Au_2P_4]^{2-}$ layer taking into account the number of bonds each atom is forming. In general, according to COHP and ELF analyses Au−Au interactions have minor contributions to the bonding in $BaAu_2P_4$.

CONCLUSIONS

The synthesis, chemical features, and physical properties of a new polyphosphide $BaAu_2P_4$ were explored. In the layered crystal structure, phosphorus polyanionic chains are condensed into $[Au_2P_4]^{2-}$ layers by means of almost linearly coordinated gold atoms. Such layers are separated by barium atoms, which are locally coordinated by 14 gold and phosphorus atoms forming a bicapped hexagonal antiprism around each Ba atom. $BaAu_2P_4$ exhibits semiconducting and diamagnetic behavior as expected from the Zintl count for this compound, $(Ba^{2+})(Au^{+})_2(P^{-})_4$. ^{31}P solid state MAS NMR confirms the presence of a single phosphorus crystallographic site and the diamagnetic nature of the compound. Static NMR reveals nearly uniaxial symmetry of the shielding tensor for the P site. Analyses of the chemical bonding by means of ELF and COHP indicate strong covalent P−P and Au−P interactions as well as the presence of electron lone pairs located on the phosphorus atoms. Au−Au interactions appear to have a minor contribution to the total bonding in the $BaAu_2P_4$. The semiconducting nature and unique crystal structure suggest the possibility of interesting thermoelectric properties. Investigations of these properties for $BaAu_2P_4$ are currently underway.

ASSOCIATED CONTENT

Supporting Information

Crystallographic data in CIF format. Further details are given in Figures SI 1−SI 5 and Table SI 1. This material is available free of charge via the Internet at http://pubs.acs.org.

AUTHOR INFORMATION

Corresponding Author

*E-mail: kkovnir@ucdavis.edu. Phone: +1-530-752-5563.

Author Contributions

The manuscript was written through contributions of all authors. All authors have given approval to the final version of the manuscript.

Notes

The authors declare no competing financial interest.

ACKNOWLEDGMENTS

This research is supported by the U.S. Department of Energy, Office of Basic Energy Sciences, Division of Materials Sciences and Engineering under Award DE-SC0008931.

REFERENCES

(1) Pöttgen, R.; Hönle, W.; von Schnering, H. G. *Encyclopedia of Inorganic Chemistry*, 2nd ed.; King, R. B., Ed.; Wiley: Chichester, U.K., 2005; Vol. *VIII*, pp 4255−4308.

(2) Hönle, W.; von Schnering, H. G. *Chem. Rev.* **1988**, *88*, 243−273.

(3) Shatruk, M. M.; Kovnir, K. A.; Shevelkov, A. V.; Popovkin, B. A. *Angew. Chem., Int. Ed.* **2000**, *39*, 2508−2509.

(4) (a) Fassler, T. F. *Struct. Bonding (Berlin, Ger.)* **2011**, *140*, 91−131. (b) Scharfe, S.; Kraus, F.; Stegmaier, S.; Schier, A.; Fassler, T. F. *Angew. Chem., Int. Ed.* **2011**, *50*, 3630−3670.

(5) (a) Lange, S.; Sebastian, C. P.; Zhang, L.; Eckert, H.; Nilges, T. *Inorg. Chem.* **2006**, *45*, 5878−5885. (b) Lange, S.; Sebastian, C. P.; Nilges, T. *Z. Anorg. Allg. Chem.* **2006**, *632*, 195−203. (c) Lange, S.; Nilges, T. *Z. Naturforsch. B* **2006**, *61*, 871−881. (d) Lange, S.; Bawohl, M.; Weihrich, R.; Nilges, T. *Angew. Chem., Int. Ed.* **2008**, *47*, 5654−5657. (e) Lincke, H.; Nilges, T.; Johrendt, D.; Pöttgen, R. *Solid State*

Sci. **2008**, *10*, 1006−1011. (f) Bawohl, M.; Nilges, T. *Z. Anorg. Allg. Chem.* **2009**, *635*, 307−311. (g) Bawohl, M.; Nilges, T. *Z. Anorg. Allg. Chem.* **2009**, *635*, 667−673. (h) Weihrich, R.; Lange, S.; Nilges, T. *Solid State Sci.* **2009**, *11*, 519−527.
(6) (a) Dewalsky, M. V.; Jeitschko, W.; Wortmann, U. *Chem. Mater.* **1991**, *3*, 316−319. (b) Eschen, M.; Wallinda, J.; Jeitschko, W. *Z. Anorg. Allg. Chem.* **2002**, *628*, 2764−2771. (c) Kaiser, P.; Jeitschko, W. *Z. Anorg. Allg. Chem.* **1996**, *622*, 53−56.
(7) (a) Eisenmann, B.; Röβler, U. *Z. Anorg. Allg. Chem.* **2003**, *629*, 459−462. (b) Chen, X.; Zhu, L.-P.; Yamanaka, S. *J. Solid State Chem.* **2003**, *173*, 449−455.
(8) Eschen, M.; Jeitschko, W. *J. Solid State Chem.* **2002**, *165*, 238−246.
(9) Dünner, J.; Mewis, A. *Z. Anorg. Allg. Chem.* **1991**, *621*, 191−196.
(10) Kovnir, K.; Stockert, U.; Budnyk, S.; Prots, Yu.; Baitinger, M.; Paschen, S.; Shevelkov, A. V.; Grin, Yu. *Inorg. Chem.* **2011**, *50*, 10387−10396.
(11) Shevelkov, A. V.; Kovnir, K. *Struct. Bonding (Berlin, Ger.)* **2011**, *139*, 97−142.
(12) *CRC Handbook of Thermoelectrics*; Rowe, D. M., Ed.; CRC Press: Boca Raton, FL, 1995.
(13) Sheldrick, G. M. *Acta Crystallogr., Sect. A* **2008**, *A64*, 112−122.
(14) Massiot, D.; Fayon, F.; Capron, M.; King, I.; Le Calve, S.; Alonso, B.; Durand, J.-O.; Bujoli, J.-O.; Gan, Z.; Hoatson, G. *Magn. Reson. Chem.* **2002**, *40*, 70−76.
(15) (a) Koepernik, K.; Eschrig, H. *Phys. Rev. B* **1999**, *59*, 1743. (b) Ophale, I.; Koepernik, K.; Eschrig, H. *Phys. Rev. B* **1999**, *60*, 14035.
(16) Perdew, J. P.; Wang, Y. *Phys. Rev. B* **1992**, *45*, 13244.
(17) Jepsen, O.; Burkhardt, A.; Andersen, O. K. *The Program TB-LMTO-ASA*, Version 4.7; Max-Planck-Institut für Festkörperforschung: Stuttgart, Germany, 1999.
(18) Dronskowski, R.; Blöchl, P. E. *J. Phys. Chem.* **1993**, *97*, 8617−8624.
(19) (a) Becke, A. D.; Edgecombe, K. E. *J. Chem. Phys.* **1990**, *92*, 5397−5403. (b) Savin, A.; Jepsen, O.; Flad, J.; Andersen, O. K.; Preuss, H.; von Schnering, H. G. *Angew. Chem., Int. Ed.* **1992**, *31*, 187−188. (c) Savin, A.; Nesper, R.; Wengert, S.; Fassler, T. F. *Angew. Chem., Int. Ed. Engl.* **1997**, *36*, 1808−1832.
(20) (a) *Paraview: Parallel visualization application*, version 3.8.1 64 bit; Sandia National Labs, Kitware Inc, Los Alamos National Labs: USA; http://paraview.org; (b) Baranov, A. I. *Visualization plugin for ParaView*, Version 3.4.11, 2012.
(21) Fulmer, J.; Kovnir. K. Unpublished results: $Ba_8Au_{16}P_{30}$ crystallizes in *Pbcn*, a = 14.6362(1) Å, b = 10.4655(1) Å, c = 28.9836(2) Å, isostructural to $Ba_8Cu_{16}P_{30}$ in ref 9.
(22) Jeitschko, W.; Möller, M. H. *Acta Crystallogr., Sect. B* **1979**, *35*, 573−579.
(23) Eisenmann, B.; Klein, J.; Somer, M. *Z. Kristallogr.* **1991**, *197*, 277−278.
(24) Nuss, J.; Jansen, M. *Z. Anorg. Allg. Chem.* **2009**, *635*, 1514−1516.
(25) Zachariasen, W. H. *Acta Crystallogr.* **1963**, *16*, 1253−1255.
(26) *Chemistry, Structure and Bonding of Zintl Phases and Ions*; Kauzlarich, S. M., Ed.; VCH: New York, 1996.
(27) Miller, G. J.; Schmidt, M. W.; Wang, F.; You, T.-S. *Struct. Bonding (Berlin)* **2011**, *139*, 1−55.
(28) Bain, G. A.; Berry, J. F. *J. Chem. Educ.* **2008**, *85*, 532−536.
(29) Kraus, F.; auf der Günne, J. S.; DiSalle, B. F.; Korber, N. *Chem. Commun.* **2006**, 218−219.
(30) auf der Günne, J. S.; Kaczmarek, S.; van Wüllen, L.; Eckert, H.; Paschke, D.; Foecker, A. J.; Jeitschko, W. *J. Solid State Chem.* **1999**, *147*, 341−349.
(31) Nissan, R. A.; Vanderah, T. A. *J. Phys. Chem. Solids* **1989**, *50*, 347−352.
(32) Wang, J.; Sen, S.; Yu, P.; Browning, N. D.; Kauzlarich, S. M. *J. Solid State Chem.* **2010**, *183*, 2522−2527.
(33) Pfannenschmidt, U.; Behrends, F.; Lincke, H.; Eul, M.; Schäfer, K.; Eckert, H.; Pöttgen, R. *Dalton Trans.* **2012**, *41*, 14188−14196.
(34) Ratai, E.; Bruins, P.; Hernandez, C. J.; Kauzlarich, S. M.; Augustine, M. P. *Chem. Mater.* **2002**, *14*, 2467−2475.
(35) Kovnir, K.; Kolen'ko, Y. V.; Baranov, A. I.; Neira, I. S.; Sobolev, A. V.; Yoshimura, M.; Presniakov, I. A.; Shevelkov, A. V. *J. Solid State Chem.* **2009**, *182*, 630−639.
(36) (a) Li, B.; Kim, S. J.; Miller, G. J.; Corbett, J. D. *Inorg. Chem.* **2009**, *48*, 6573−6583. (b) Li, B.; Kim, S. J.; Miller, G. J.; Corbett, J. D. *Inorg. Chem.* **2009**, *48*, 11108−11113. (c) Li, B.; Kim, S. J.; Miller, G. J.; Corbett, J. D. *Inorg. Chem.* **2010**, *49*, 1503−1509. (d) Smetana, V.; Lin, Q. S.; Pratt, D. K.; Kreyssig, A.; Ramazanoglu, M.; Corbett, J. D.; Goldman, A. I.; Miller, G. J. *Angew. Chem., Int. Ed.* **2012**, *51*, 12699−12702. (e) Smetana, V.; Corbett, J. D.; Miller, G. J. *Inorg. Chem.* **2012**, *51*, 1695−1702. (f) Smetana, V.; Corbett, J. D.; Miller, G. J. *Inorg. Chem.* **2012**, *51*, 7711−7721.
(37) Kim, S. J.; Miller, G. J.; Corbett, J. D. *Z. Anorg. Allg. Chem.* **2010**, *636*, 67−73.